

DeSplat: Decomposed Gaussian Splatting for Distractor-Free Rendering

Yihao Wang¹, Marcus Klasson², Matias Turkulainen², Shuzhe Wang², Juho Kannala^{2,3}, Arno Solin²
¹Technical University of Munich ²Aalto University ³University of Oulu
 johanna.wang@tum.de {firstname.lastname}@aalto.fi

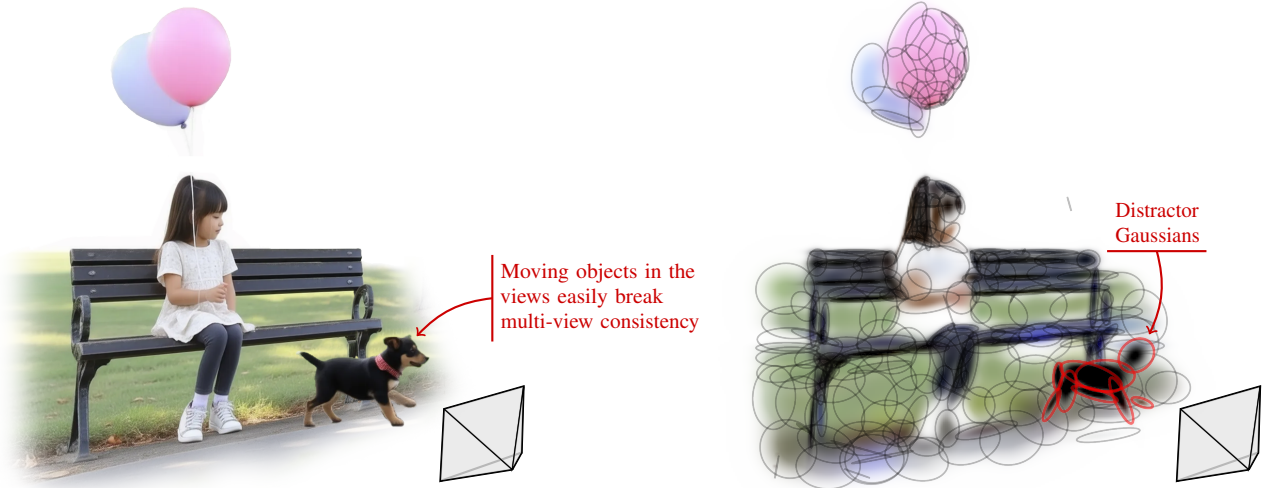


Figure 1. **DeSplat**: Gaussian Splatting struggles with floaters and artifacts when image sequences violate photometric consistency assumptions. Unlike existing distractor-free methods which rely on external semantic features, we propose a fully splatting-based solution grounded in photometric consistency that decomposes 3DGS scenes into static components and per-view distractors.

Abstract

Gaussian splatting enables fast novel view synthesis in static 3D environments. However, reconstructing real-world environments remains challenging as distractors or occluders break the multi-view consistency assumption required for accurate 3D reconstruction. Most existing methods rely on external semantic information from pre-trained models, introducing additional computational overhead as pre-processing steps or during optimization. In this work, we propose a novel method, DeSplat, that directly separates distractors and static scene elements purely based on volume rendering of Gaussian primitives. We initialize Gaussians within each camera view for reconstructing the view-specific distractors to separately model the static 3D scene and distractors in the alpha compositing stages. DeSplat yields an explicit scene separation of static elements and distractors, achieving comparable results to prior distractor-free approaches without sacrificing rendering speed. We demonstrate DeSplat’s effectiveness on three benchmark data sets for distractor-free novel view synthesis. See the project website at <https://aaltoml.github.io/desplat/>.

1. Introduction

3D Gaussian Splatting (3DGS, [8]) is a popular framework for novel view synthesis for its fast rendering and training speeds with high-quality results. However, learning accurate scene reconstructions with 3DGS from images of non-static scenes containing distractors [12, 25, 28]—e.g., moving people, vegetation, or transient effects [17] remains challenging. Vanilla 3DGS is optimized to satisfy a static volumetric rendering constraint even though reference images can contain multi-view inconsistent distractors. This results in spurious floaters being generated close to camera views or as thin view-specific effects appearing in only a few views. This lack of robustness limits applying 3DGS to unstructured image collections, e.g. crowd-sourced images [31], and casually captured videos [22, 37].

Prior work in 3DGS and Neural Radiance Fields (NeRFs, [18]) for distractor-free rendering aim to detect which pixels in reference images belong to distractors and to reduce their influence during optimization. RobustNeRF [28] computes robust masks that detect where distractors are present in images from pixel residuals and weight the reconstruction

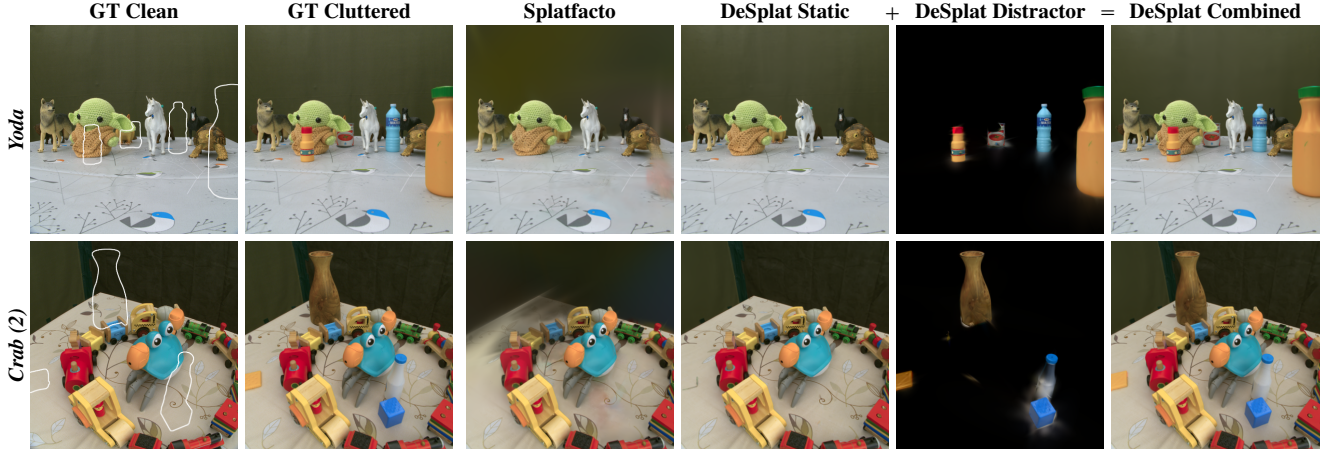


Figure 2. **Qualitative visualization of static and distractor elements achieved by our method, DeSplat (Sec. 3.1).** In the *Yoda* and *Crab (2)* scenes [28], both clean and cluttered images are captured from the same viewpoints. By explicitly modeling the scene using static and distractor Gaussians, our approach enables clear distractor segmentation and reduced artifacts compared to the Splatfacto baseline [33].

loss accordingly. The same approach has recently been applied to 3DGS where pre-trained networks are utilized for improving the learned masks [13, 29]. However, it is currently under-explored how the errors from the pre-trained networks affect the 3DGS framework, especially in the densification step [8, 13]. Furthermore, recent works closely follow NeRF-W [17] and introduce separate networks for modeling transient effects which introduces additional computational cost resulting in lower rendering speeds [6, 13, 45]. It remains an open question if the 3DGS inverse rendering framework could be modified to directly recognize what portions of reference images belong to a static scene and what belong to spurious distractors.

In this paper, we propose decomposing the 3D scene representation into two distinct sets of Gaussian primitives responsible for reconstruction the underlying static scene and distractors respectively. Our approach named DeSplat involves initializing distractor Gaussians for per-view transient effects which are jointly optimized with the static scene (see Fig. 1). The explicit modeling of transient and static Gaussians allows decomposing the volumetric rendering equation into two portions and separate optimization into learning per-view transient effects and the static 3D scene utilizing the same photometric reconstruction loss as proposed in Kerbl *et al.* [8]. See Fig. 2 for a demonstration. This separation maintains the same fast rendering capabilities without introducing additional pre-processing steps.

Contributions Our contributions can be summarized as:

- We propose decomposing the 3DGS image formation model and training objective to explicitly learn both transient per-view distractors and the static scene relying only on photometric supervision.
- Our approach is efficient and entirely splatting-based allowing for effective robustification of 3DGS which is fully

compatible with existing 3DGS tools and pipelines.

- We perform experiments on RobustNeRF [28], On-the-go [25], and Photo Tourism [31] data sets containing confounding distractors and show that our decomposed 3DGS method performs well against baselines that require pre-trained networks for detecting distractors.

2. Related Work

Robustness in the Presence of Distractors Novel view synthesis from non-static images is an active research area. Early attempts have aimed to separate static scene elements from transient parts [17] and occluders [28] using photometric-based loss functions. For NeRF-based approaches, NeRF-W [17] uses separate MLPs to model static and transient components, applying weights to the per-pixel reconstruction loss based on uncertainty estimates. Other methods utilize learned visibility masks [5, 42] to modulate the reconstruction loss. RobustNeRF [28] introduces a kernel-based robust estimator, trained with iteratively re-weighted least squares, to detect distractors using photometric error for loss weighting. Recently, pre-trained models [11, 20] have been adopted to enhance occluder detection through semantic cues. NeRF On-the-go [25] refines the pixel-wise loss using an uncertainty predictor trained with DINOv2 [20] features, while NeRF-HuGS [3] learns static maps based on SfM features and segmentation from SAM [11].

Several 3DGS-based methods that are robust to distractors have also been introduced. SpotlessSplats [29] uses semantic features from Stable Diffusion [26, 34] for spatial and spatio-temporal clustering combined with robust masking to identify distractors. WildGaussians [13] predicts uncertainty similarly as [25], but computes a binary mask from the uncertainties for gradient scaling to stabilize optimization. For unstructured photo collections, Splatfacto-

Table 1. **Comparison to prior art.** We briefly summarize prior methods based on three criteria: need for external pre-trained models for feature or segmentation generation, rendering performance compared to the original 3DGS work [8], and explicit scene separation. Explicit scene separation refers to the ability to distinctly separate a scene into static and transient distractor elements.

| | SWAG [6] | GS-W [45] | Wild-GS [40] | Splatfacto-W [39] | WildGaussians [13] | SpotlessSplats [29] | DeSplat (ours) |
|---------------------------|----------|-----------|--------------|-------------------|--------------------|---------------------|----------------|
| No pre-trained model | ✓ | × | × | ✓ | × | × | ✓ |
| Fast 3DGS rendering speed | × | × | × | ✓ | ✓ | ✓ | ✓ |
| Explicit scene separation | × | × | × | × | × | × | ✓ |

W [39] uses MLPs for appearance and background modeling combined with robust masks for handling transient effects and objects, SWAG [6] predicts per-Gaussian opacity shifts with an MLP combined with image-conditioned embeddings, while [40, 45] learns visibility masks with a U-Net [27] and feature embeddings for static and transient object handling. The methods mentioned above require neural networks to model transient effects and occluders, either with pre-trained models [13, 29] or learning feature embeddings [6, 39, 40, 45] during optimization, which introduce additional computational costs. In contrast, we propose a purely splatting-based framework that learns to reconstruct static and distractor objects separately by decomposing the volume-rendering function and minimizing the photometric loss from 3DGS [8].

Scene Decomposition Learning scene decomposition of static and dynamic objects is an active field in computer vision and graphics [44], where generative models have been popular for single- and multi-object decomposition [1, 4, 15, 16, 19]. Several composite radiance fields for decoupling static and dynamic elements have been proposed with NeRFs [14, 38] and 3DGS [43, 47] learned from monocular video. Large-scale novel view synthesis with NeRF and 3DGS in urban scenes have incorporated scene semantics [21, 24, 32] and 3D bounding boxes [35, 41, 48] to specify moving objects. Moreover, separate modeling of backgrounds to disentangle static objects from lighting and weather conditions have been proposed [13, 17, 39]. In this paper, we propose a decomposition of 3DGS where two sets of Gaussian points are used for fitting the static elements and distractors separately. We draw inspiration from representing 2D images with Gaussian Splatting [46] and initialize view-specific Gaussian points for modeling per-view distractors near the camera plane.

Comparison to Previous Methods In Table 1, we present

the main differences between our proposed method and previous works. Our method relies solely on volume rendering and a photometric loss, without the need for introducing additional neural networks. GS-W and Wild-GS on the other hand use a pre-trained ResNet-18 [7] for encoding appearance features and WildGaussians and SpotLessSplats use features from foundation models [20, 26] for detecting distractors. However, our method is still fully compatible with prior approaches using neural networks for modeling scene appearance [13, 29], background [39], and/or distractors due to its generality. Regarding rendering speed, our method achieves similar speed as 3DGS since Gaussians are rasterized directly without having to cache image features to maintain fast rendering [40, 45] times. Finally, we achieve explicit scene separation between the underlying static scene and distractor elements by decomposing 3DGS, whilst previous methods aim to mitigate overfitting to distractors via loss masking by detecting distractor pixels from the reference images. Instead, our method jointly reconstructs distractor elements, rather than simply masking them.

3. Methods

3D Gaussian splatting [8] represents a scene with a set of 3D Gaussian points \mathcal{G} . Each Gaussian point are associated with a position $\boldsymbol{\mu} \in \mathbb{R}^3$, covariance matrix $\boldsymbol{\Sigma} \in \mathbb{R}^{3 \times 3}$, opacity $o \in [0, 1]$, and view-dependent color \mathbf{c} parameterized by spherical harmonics (SH) coefficients.

When rendering images, Gaussian points are splatted into screen space as 2D Gaussians with means $\boldsymbol{\mu}' \in \mathbb{R}^2$ obtained via projective transformation and covariances approximated by $\boldsymbol{\Sigma}' = \mathbf{J}\mathbf{W}\boldsymbol{\Sigma}\mathbf{W}^\top\mathbf{J}^\top \in \mathbb{R}^{2 \times 2}$ where $\mathbf{J} \in \mathbb{R}^{2 \times 3}$ is the Jacobian of the first-order Taylor approximation of the projective transformation, and $\mathbf{W} \in \mathbb{R}^{3 \times 3}$ is the view transformation. The Gaussians overlapping with the target pixel are sorted according to depth and rendered using alpha-blending:

$$\mathbf{c}_{\text{GS}} = \sum_{i=1}^N \mathbf{c}_i \alpha_i \prod_{j=1}^{i-1} (1 - \alpha_j), \quad (1)$$

$$\alpha_i = o_i \cdot \exp\left(-\frac{1}{2} \Delta_i^\top \boldsymbol{\Sigma}'^{-1} \Delta_i\right), \quad (2)$$

where N is the number of depth-sorted Gaussians, α denotes alpha-blending weights and $\Delta_i = (\mathbf{x}'_i - \boldsymbol{\mu}'_i)$ is the offset between the pixel center \mathbf{x}'_i and the 2D Gaussian mean $\boldsymbol{\mu}'_i$. Gaussian points are optimized by minimizing the following reconstruction loss between rendered pixels and ground truth reference images:

$$\mathcal{L}_{\text{GS}} = (1 - \lambda) \mathcal{L}_1 + \lambda \mathcal{L}_{\text{D-SSIM}}, \quad (3)$$

where \mathcal{L}_1 is an L_1 loss, $\mathcal{L}_{\text{D-SSIM}}$ is a SSIM [36] loss, and λ is a weighting factor.

The Gaussian points are initialized using a sparse point cloud obtained from a Structure-from-Motion approach, *e.g.*,

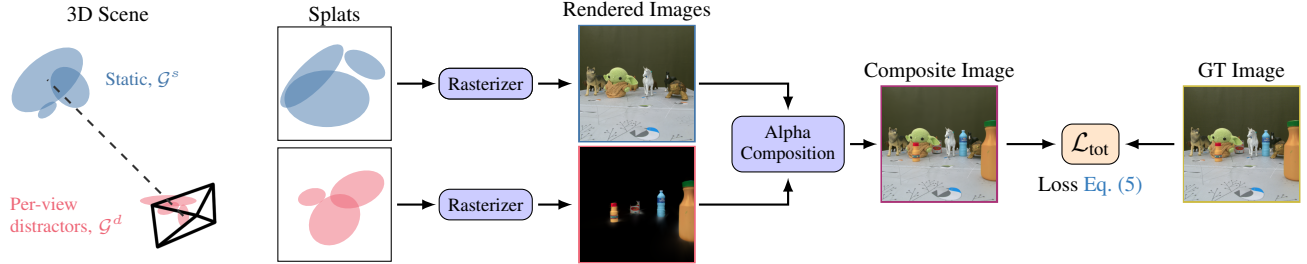


Figure 3. **Method overview:** We decompose 3DGS to model the static scene and per-view distractors explicitly. The static scene \mathcal{G}^s is optimized for all camera-views but we allow learning of per-view distractor Gaussians \mathcal{G}^d to model spurious transient effects which are jointly optimized with the static scene via alpha-compositing. We show how this formulation allows implicit learning of distractor segmentation masks and decomposition of the 3DGS scene into static and distractor elements.

COLMAP [30]. Gaussians are densified via Adaptive Density Control (ADC, [8]) that performs cloning of Gaussians in under-reconstructed regions and splitting large Gaussians in over-reconstructed parts of the scene.

3.1. Decomposed 3D Gaussian Splatting

We propose decomposing the 3DGS representation to model the static scene and distractors explicitly. The idea is to initialize two sets of Gaussian points \mathcal{G}_s and \mathcal{G}_d , which are optimized to reconstruct the static scene and distractors respectively. We render images using volume rendering [23] (ref. Eq. (1)) by decomposing the output pixel color for a given view into two distinct blended images, one for the static scene and one for distractors using

$$\mathbf{c}_{\text{comp}} = \mathbf{c}_d + (1 - \alpha_d)\mathbf{c}_s \text{ and } \alpha_d = \sum_{i=1}^{N_d} \alpha_{d,i} \prod_{j=1}^{i-1} (1 - \alpha_{d,j}), \quad (4)$$

where \mathbf{c}_d and \mathbf{c}_s are alpha-composited colors pre-multiplied with alpha-blending weights for the distractor and static Gaussians respectively. α_d represents the blending weight of the N_d distractor Gaussians overlapping with the target pixel. This separation allows rendering the static scene elements and distractors independently.

Per-view Distractor Gaussians Decomposing a scene into static and distractor Gaussians is challenging when distractors appear in several views or shift slightly between frames. A globally shared set of distractor Gaussians may not be effective since distractors often behave as view-dependent effects. Therefore, we initialize a set of distractor Gaussians for each n -th view as $\mathcal{G}_{d,n}$ where $n = 1, \dots, N_{\text{train}}$ and N_{train} is the total number of training images. The per-view distractor Gaussians are optimized only when the associated camera view is selected during optimization.

Initialization of Distractor Gaussians We initialize the locations of the distractor Gaussians per-view by placing them on a 2D plane in-front of camera views. For a single view

with camera-to-world rotation matrix \mathbf{R} and translation vector \mathbf{t} , the distractor Gaussian positions are initialized as $\boldsymbol{\mu}^d = \mathbf{t} - \mathbf{R}^\top \mathbf{u}$, where $\mathbf{u} = [\rho u, \rho v, \rho]^\top$. Here, $u, v \sim \mathcal{U}(0, 1)$ are sampled from a uniform distribution, and the constant ρ controls the depth, with $\rho = 0.02$ performing well in our experiments. Other Gaussian parameters follow the standard initialization from 3DGS [8]. A fixed number of distractor Gaussians are initialized for each training camera view.

Per-view Densification We apply Adaptive Density Control (ADC, [8]) to the per-view distractor Gaussians to handle varying number and area of distractors in the training images. Unlike the ADC in 3DGS that densifies Gaussian points after every T iteration, we densify the distractor Gaussians when their corresponding image has been trained S times. The culling, splitting, and duplication procedures are the same as in 3DGS for both the distractor and static Gaussians.

Method Pipeline Fig. 3 gives an overview of the rasterization and loss computation of DeSplat. The static Gaussian points are initialized globally using the sparse point cloud obtained from COLMAP as commonly done in 3DGS [8], whereas distractor Gaussian points are initialized locally in front of each camera view. The static and view-specific distractor Gaussians are splatted onto the screen space and rasterized separately with Eq. (1) to render two images representing the static elements and distractors respectively. We obtain a composite image via alpha-composition of the two images as in Eq. (4), which is compared against the ground-truth image to compute a photometric loss. By reconstructing both static elements and distractors, we obtain an explicit scene separation that allows rendering the static and distractor components independently.

Loss Function We apply regularization on the opacities and alpha maps of the distractor Gaussians to enhance the distractor separation. The idea is to reconstruct the distractors with as few Gaussians as possible, which has previously been applied to balance memory and compute in 3DGS [9, 12].

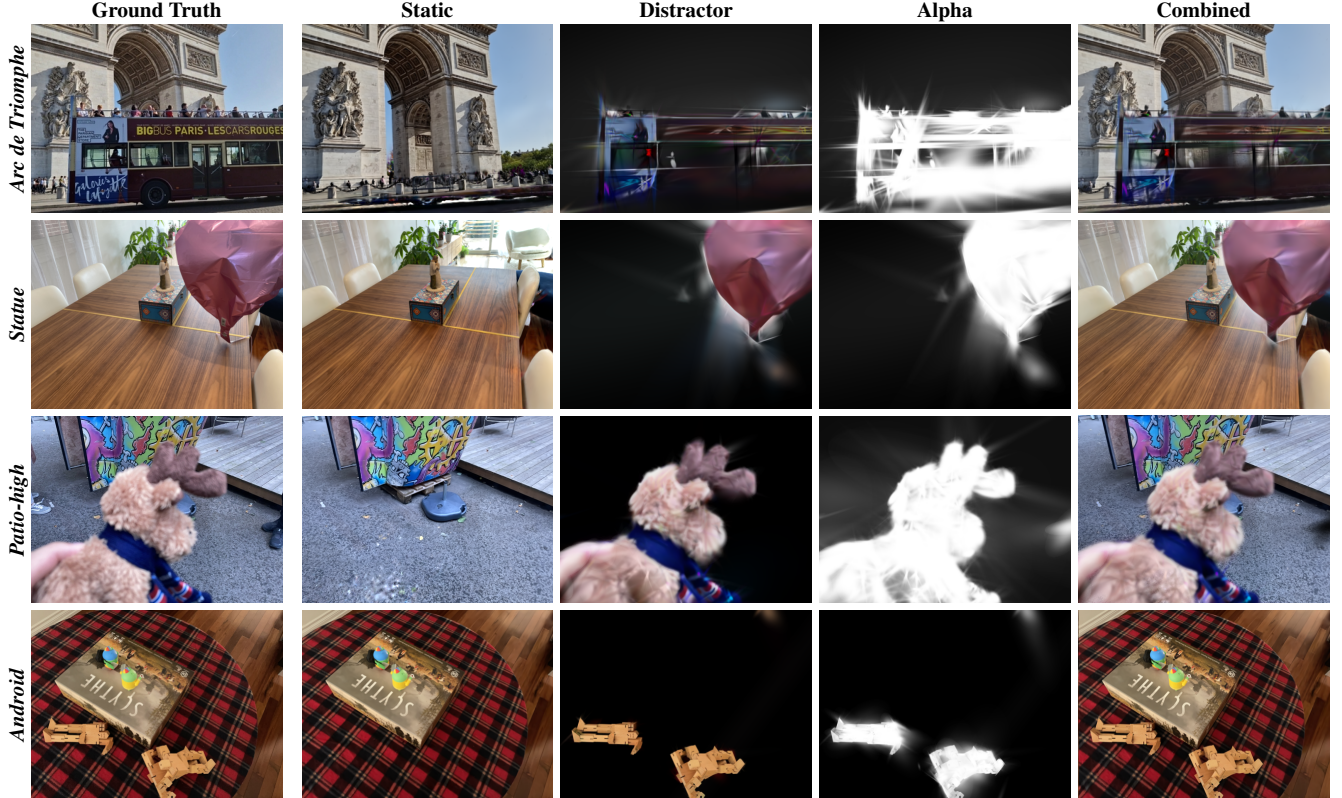


Figure 4. **Handling occluders.** Examples of static and transient components alongside the composited images. The transient components exhibit well-defined boundaries, while the quality of the static scene is preserved. This showcases the ability of our model to learn transient components without requiring semantic supervision or external priors from pre-trained networks.

The final loss function is defined as

$$\mathcal{L}_{\text{tot}} = \mathcal{L}_{\text{GS}} + \lambda_s |1 - \alpha_s| + \lambda_d |\alpha_d| \quad (5)$$

where the second and third terms are L_1 regularizers on the static and distractor blending weights α_s and α_d with multipliers λ_d and λ_s , respectively. These terms discourage the model from using distractor Gaussians to explain static objects and encourage the accumulation of static Gaussians being equal to one, thereby reducing the likelihood of holes in the background.

4. Experiments

We conduct experiments on the data sets RobustNeRF [28], On-the-go [25], and Photo Tourism [31] to evaluate the efficacy and robustness of our method across varying occlusion and scene complexities. The experiments show DeSplat’s ability to handle occluders and background separation, emphasizing performance in cluttered and open scenes under dynamic lighting conditions. In Sec. 4.1, we benchmark our method against state-of-the-art NeRF- and 3DGS-based baselines, assessing both qualitative and quantitative outcomes. Sec. 4.2 presents ablation studies to validate the

impact of core model components on occluder handling and scene reconstruction.

Data Sets We evaluate our method using the RobustNeRF [28], On-the-go [25], and Photo Tourism [31] data sets. For RobustNeRF, we evaluate on all five available scenes *Statue*, *Android*, *Crab (1)*, *Crab (2)*, and *Yoda*, and downscale all images $8\times$ [28]. For On-the-go, we evaluate on the scenes *Mountain*, *Fountain*, *Corner*, *Patio*, *Spot*, and *Patio-High*, where all images are downscaled $8\times$ except the *Patio* scene which is downscaled $4\times$ [25]. Moreover, we use *Arc de Triomphe* for visualization (see Fig. 4). To validate the effectiveness of our proposed method and its compatibility with prior approaches, we also evaluate on the *Brandenburg Gate*, *Sacre Coeur*, and *Trevi Fountain* scenes from the Photo Tourism data set.

Baselines We compare DeSplat against state-of-the-art 3DGS-based approaches for distractor-free rendering, such as SpotlessSplats [29] (SLS-mlp) and WildGaussians [13], as well as Splatfacto [33] which serves as our vanilla 3DGS baseline. For RobustNerf and On-the-go scenes, we also run Splatfacto-W-A with appearance embeddings and its extension with robust mask for distractor detection called

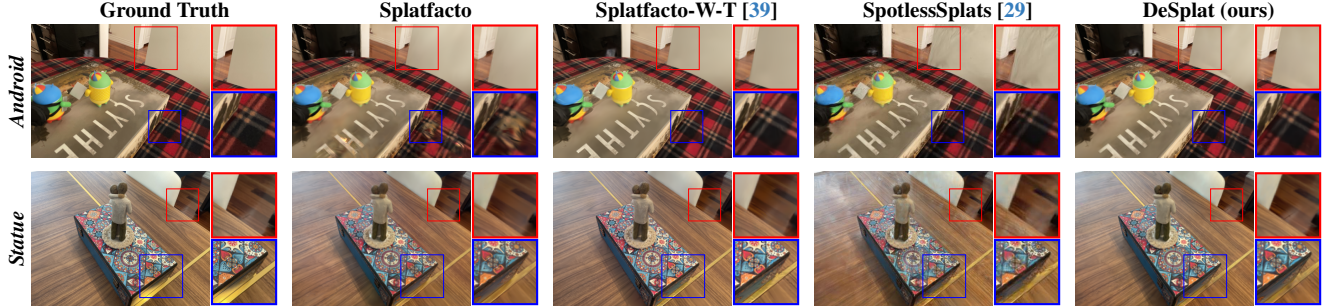


Figure 5. **Qualitative results on the RobustNeRF data set [28].** In the *Android* and *Statue* scenes, DeSplat generates fewer artefacts than Splatfacto and reconstructs static objects and backgrounds accurately. More qualitative examples in Fig. A10 in the Appendix.

Table 2. **Performance comparison between our method and the baselines on the RobustNeRF data set [28].** The **first**, **second**, and **third** best values are highlighted. * denotes that the reported baseline was ran by us, and ‘-’ denotes that the metric is missing in the corresponding work. The explicit scene separation from our DeSplat achieves the best performance on most scenes.

| Method | <i>Statue</i> | | | <i>Android</i> | | | <i>Crab (1)</i> | | | <i>Crab (2)</i> | | | <i>BabyYoda</i> | | |
|-----------------------|-----------------|-----------------|--------------------|-----------------|-----------------|--------------------|-----------------|-----------------|--------------------|-----------------|-----------------|--------------------|-----------------|-----------------|--------------------|
| | PSNR \uparrow | SSIM \uparrow | LPIPS \downarrow | PSNR \uparrow | SSIM \uparrow | LPIPS \downarrow | PSNR \uparrow | SSIM \uparrow | LPIPS \downarrow | PSNR \uparrow | SSIM \uparrow | LPIPS \downarrow | PSNR \uparrow | SSIM \uparrow | LPIPS \downarrow |
| RobustNeRF [28] | 20.89 | 0.75 | 0.28 | 21.72 | 0.65 | 0.31 | 30.75 | 0.81 | 0.21 | - | - | - | 30.87 | 0.83 | 0.20 |
| NeRF On-the-go [25] | 21.58 | 0.77 | 0.24 | 23.50 | 0.75 | 0.21 | - | - | - | - | - | - | 29.96 | 0.83 | 0.24 |
| NeRF-HuGS [3] | 21.00 | 0.77 | 0.13 | 23.32 | 0.76 | 0.12 | 34.16 | 0.96 | 0.03 | - | - | - | 30.70 | 0.83 | 0.12 |
| Splatfacto* [33] | 22.75 | 0.87 | 0.11 | 24.46 | 0.83 | 0.09 | 24.80 | 0.92 | 0.13 | 31.20 | 0.94 | 0.11 | 32.91 | 0.96 | 0.09 |
| Splatfacto-W-A* [39] | 22.63 | 0.88 | 0.10 | 24.18 | 0.83 | 0.09 | 25.06 | 0.92 | 0.15 | 31.93 | 0.95 | 0.09 | 29.28 | 0.96 | 0.09 |
| Splatfacto-W-T* [39] | 23.21 | 0.89 | 0.09 | 25.39 | 0.87 | 0.07 | 28.74 | 0.95 | 0.09 | 24.41 | 0.91 | 0.19 | 31.53 | 0.96 | 0.08 |
| SLS-mlp [29] | 22.69 | 0.85 | 0.12 | 25.15 | 0.86 | 0.09 | 35.85 | 0.97 | 0.08 | 34.35 | 0.96 | 0.03 | 33.60 | 0.96 | 0.10 |
| DeSplat (ours) | 23.40 | 0.88 | 0.10 | 24.80 | 0.85 | 0.08 | 36.15 | 0.97 | 0.04 | 35.23 | 0.96 | 0.07 | 35.60 | 0.96 | 0.06 |

Splatfacto-W-T [39] with their textilight hyperparameter setup. On the RobustNeRF scenes, we include from the distractor-free NeRF methods RobustNeRF [28], NeRF On-the-go [25], and NeRF-HuGS [3]. For Photo Tourism, we compare against SWAG [6], GS-W [45], Wild-GS [40], Splatfacto-W [39], and WildGaussians [13]. To ensure consistency, we show the reported PSNR, SSIM, and LPIPS metrics from the corresponding works to compare against the performance of our DeSplat.

Implementation Details We follow the hyperparameter settings for Splatfacto [33] and train for 30k iterations on the RobustNeRF and On-the-go scenes. The static Gaussian points are configured using the standard initialization and update procedure for Splatfacto. We initialize $K = 1000$ distractor points in every training image using the procedure described in Sec. 3.1. The gradients of the distractor points are logged for ADC, which is performed for the distractor points in every image after all images has been seen $S = 10$ times. All parameters of the distractor points are optimized using Adam [10]. Increasing the learning rate by $10\times$ was necessary for the quaternions and scales, while the learning rates for the means, opacities and colors are kept as default. We model the color of distractors directly with three-dimensional RGB vectors instead of relying on SH coefficients, since the distractor points are per-view which alleviates the need for compensating for view-dependent

effects using SH. We also disable the opacity reset [8] for distractor Gaussians as this improved the separation of distractors from static objects. Additionally, we apply clamping of the RGB colors instead of using a sigmoid function [33], which enabled better learning of distractors with colors at the extremes white (1) and black (0). The regularization weights λ_d and λ_s are set to 0.01.

For the PhotoTourism data set, we integrate appearance learning as described in WildGaussians [13] and background modeling following Splatfacto-W [39]. Test-time optimization [13, 17] is employed to learn the appearance embeddings of test images. Due to the larger number of input images compared to the RobustNeRF and On-the-go data sets, we adjust the learning rate and other parameters accordingly. See App. B for more details and hyperparameter values.

4.1. Distractor-free 3D Reconstruction

Comparison on RobustNeRF Data Set [28] Table 2 shows the performance metrics for our DeSplat and the baselines. We observe that DeSplat performs the best or on par with the baselines across all scenes, especially on the *Yoda* and *Crab* scenes where the distractors are removed and/or new distractors are introduced for every image. On *Statue* and *Android* scenes, DeSplat perform similarly to the best baselines Splatfacto-W-T and SLS-mlp without introducing MLPs for modeling varying appearances and lighting changes between

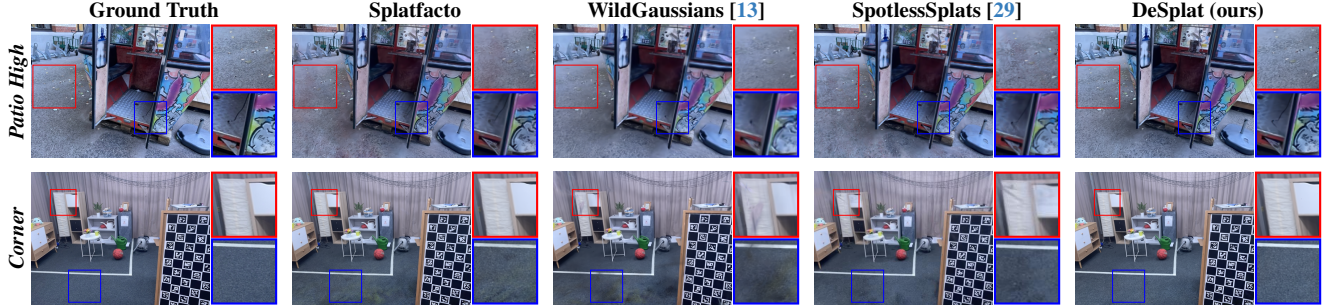


Figure 6. Qualitative results on NeRF On-the-go (*Patio High* and *Corner*) data set. More examples in Fig. A11 in the Appendix.

Table 3. Performance comparison between our method and the baselines on the On-the-go data set [25]. The first, second, and third best values are highlighted. * denotes that the reported baseline was ran by us. Our method performs the best or on par with the baselines for the scenes with medium and high occlusion rate, but struggles with modeling outdoor scenes like the *Mountain* and *Fountain* scenes.

| Method | Low Occlusion | | | | | | Medium Occlusion | | | | | | High Occlusion | | | | | |
|-----------------------|-----------------|-----------------|--------------------|-----------------|-----------------|--------------------|------------------|-----------------|--------------------|-----------------|-------------------|--------------------|-----------------|-----------------|--------------------|-----------------|-----------------|--------------------|
| | <i>Mountain</i> | | <i>Fountain</i> | | <i>Corner</i> | | <i>Patio</i> | | <i>Spot</i> | | <i>Patio-High</i> | | | | | | | |
| | PSNR \uparrow | SSIM \uparrow | LPIPS \downarrow | PSNR \uparrow | SSIM \uparrow | LPIPS \downarrow | PSNR \uparrow | SSIM \uparrow | LPIPS \downarrow | PSNR \uparrow | SSIM \uparrow | LPIPS \downarrow | PSNR \uparrow | SSIM \uparrow | LPIPS \downarrow | PSNR \uparrow | SSIM \uparrow | LPIPS \downarrow |
| NeRF On-the-go [25] | 20.15 | 0.64 | 0.26 | 20.11 | 0.61 | 0.31 | 24.22 | 0.81 | 0.19 | 20.78 | 0.75 | 0.22 | 23.33 | 0.79 | 0.19 | 21.41 | 0.72 | 0.24 |
| Splatfacto* [33] | 21.08 | 0.72 | 0.16 | 20.62 | 0.68 | 0.17 | 25.37 | 0.88 | 0.09 | 18.06 | 0.74 | 0.18 | 23.73 | 0.85 | 0.15 | 21.68 | 0.78 | 0.21 |
| Splatfacto-W-A* [39] | 20.31 | 0.69 | 0.21 | 18.74 | 0.64 | 0.21 | 25.18 | 0.86 | 0.11 | 17.92 | 0.69 | 0.20 | 23.29 | 0.82 | 0.21 | 20.68 | 0.74 | 0.26 |
| Splatfacto-W-T* [39] | 20.94 | 0.70 | 0.20 | 19.20 | 0.65 | 0.20 | 26.15 | 0.89 | 0.08 | 18.57 | 0.73 | 0.17 | 23.80 | 0.85 | 0.15 | 22.05 | 0.77 | 0.22 |
| SLS-mlp [29] | 22.53 | 0.77 | 0.18 | 22.81 | 0.80 | 0.15 | 26.43 | 0.90 | 0.10 | 22.24 | 0.86 | 0.10 | 25.76 | 0.90 | 0.12 | 22.84 | 0.83 | 0.16 |
| WildGaussians [13] | 20.43 | 0.65 | 0.26 | 20.81 | 0.66 | 0.22 | 24.16 | 0.82 | 0.05 | 21.44 | 0.80 | 0.14 | 23.82 | 0.82 | 0.14 | 22.23 | 0.73 | 0.21 |
| DeSplat (ours) | 19.59 | 0.71 | 0.17 | 20.27 | 0.68 | 0.17 | 26.05 | 0.88 | 0.09 | 20.89 | 0.81 | 0.11 | 26.07 | 0.90 | 0.09 | 22.59 | 0.84 | 0.12 |

the images.

In Fig. 5, we show qualitative examples of DeSplat and the best baselines on the *Statue* and *Android* scenes. We observe that DeSplat removes distractors effectively to preserve fine details within the static scene elements and renders more accurate backgrounds, as highlighted in the zoom-in boxes. In the *Statue* scene, DeSplat not only reconstructs details more accurately but also generates fewer artifacts compared to Splatfacto and SpotlessSplats. Nevertheless, the explicit scene separation by DeSplat achieves accurate reconstruction of the static elements in the scenes and can handle scenes with multiple distractors of various appearances effectively.

Comparison on On-the-go Data Set [25] Table 3 shows the performance metrics for our DeSplat and the baselines, where our method performs the best or on par with the baselines for the scenes with medium and high occlusion rate. However, DeSplat struggles with modeling outdoor scenes *Mountain* and *Fountain* scenes with low occlusion rates, where the distractor Gaussians often confuses the sky as a moving distractor between views. This typically results in small holes in the rendered images from static Gaussians which in turn penalizes the PSNR severely (see App. B.6 for examples). Despite this challenge, our method perform well on the SSIM and LPIPS metrics, which indicates that DeSplat manages to capture structural and perceptual aspects in its reconstructions of these scenes.

Fig. 6 shows visual examples of DeSplat and the best baselines on the *Patio High* and *Corner* scenes. In *Patio*

High, our DeSplat and WildGaussians effectively remove floaters arising from the moving people and toys in the training images, while Splatfacto and SpotlessSplats render red artefacts on the floor. By closer inspection of the door of the cabin, we observe that DeSplat manages to reconstruct fine details better than the other baselines in this scene. We do the same observation in the *Corner* scene where DeSplat produces more crisp reconstructions of fine details of static objects compared to SpotLessSplats and WildGaussians. Despite being a pure splatting method, DeSplat often achieve accurate separation of people distractors in these real-world scenes.

Comparison on Photo Tourism Data Set [31] Even in the challenging PhotoTourism data set, which features large variations in appearance and exposure between frames, our method effectively separates occluders from static objects while successfully leveraging appearance embeddings, as shown in Fig. 7. Quantitative results after test-time optimization, following the protocol described in WildGaussians [13], are provided in the supplementary materials App. B.

4.2. Ablation Studies

Ablation of Our Components We conduct an ablation study on the *Statue* and *Android* scenes [28] to evaluate different components of our method: enabling distractor Gaussians, applying ADC to them, and using our opacity regularization terms. Table 4 shows the metrics, with Splatfacto [33] as the baseline (all components off). The results



Figure 7. **Qualitative results on Photo Tourism with appearance modeling.** We enable per-view appearance modeling following prior approaches [2, 13, 17, 29] and our method still effectively separates the static and transient components, whilst learning inter-frame appearance variations.

Table 4. **Quantitative ablation on Statue and Android [28].** We compare the impact of various components of our approach.

| Distractor Gaussians | ADC | Regularization | Statue | | | Android | | |
|----------------------|-----|----------------|--------|------|-------|---------|------|-------|
| | | | PSNR | SSIM | LPIPS | PSNR | SSIM | LPIPS |
| × | × | × | 22.75 | 0.87 | 0.11 | 24.46 | 0.83 | 0.09 |
| ✓ | × | × | 21.37 | 0.85 | 0.10 | 22.92 | 0.81 | 0.10 |
| ✓ | ✓ | × | 23.52 | 0.88 | 0.10 | 24.69 | 0.84 | 0.08 |
| ✓ | ✓ | ✓ | 23.40 | 0.88 | 0.10 | 24.80 | 0.84 | 0.08 |

emphasize the importance of our choices. Qualitative results in Fig. 8 show finer separation with ADC and regularization. Without ADC, the performance is slightly lower compared to Splatfacto [33], as the redundant distractor Gaussians cannot be pruned, leading to challenges in balancing with static Gaussians. While regularization slightly reduces PSNR, it avoids over-explanation of static objects, resulting in better separation as seen in the renders (right-side image, Fig. 8).

In App. B.5, we also compare the effects of different initialization methods, memory usage, rendering speed (FPS), and training times between our method and other approaches. Compared to Splatfacto, the addition of distractor Gaussians results in only a slight increase in memory usage, whilst maintaining nearly identical rendering speeds. Compared with SpotlessSplats [29] and WildGaussians [40], our method not only reduces the time required for training, but exhibits superior memory efficiency and rendering speed.

Sensitivity Not all views in real-world scenes contain occluders. The RobustNeRF data set [28] includes both clean and cluttered data from the same viewpoints, enabling robustness testing by adjusting the ratio of cluttered images. We ablate the performance of our method with different clutter ratios in Fig. 9. With ADC enabled for our distractor Gaussians, we demonstrate robustness to various clutter ratios. We notice a significant drop in performance for the Splatfacto baseline when distractor ratio is increased, whilst our method maintains comparable metrics. In Fig. 9, we also ablate the number of initialized distractor Gaussians with ADC enabled and find that we reach best performance and saturation with only 1k Gaussians per view.

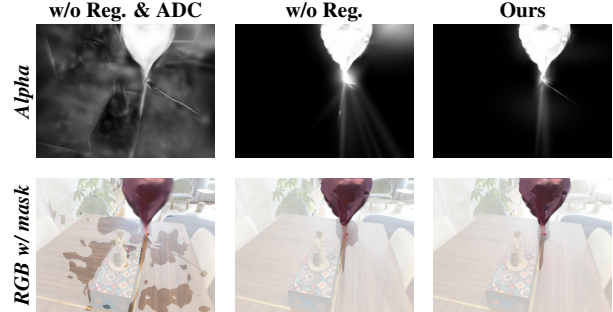


Figure 8. **Qualitative Ablation on Statue [28].** Results without both regularization (Reg.) and Adaptive Density Control (ADC), without regularization but with ADC, and ours.

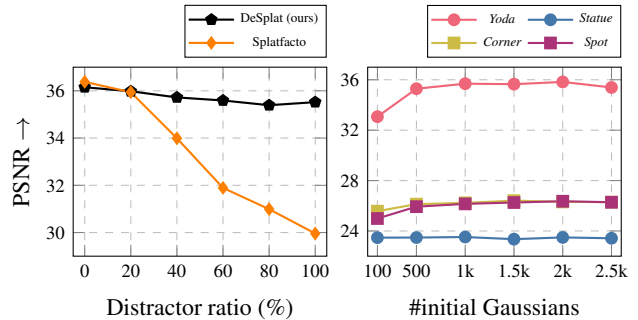


Figure 9. **Ablation study on sensitivity.** (left) PSNR for DeSplat and Splatfacto on *Yoda* scene over various ratios of distractors. (right) PSNR for DeSplat with different number of initialized distractor Gaussians per view. DeSplat performs robustly over different distractor ratios with saturation after 1000 initialized points.

5. Conclusions

We have introduced DeSplat, a novel method that separates occluders from static scene elements using volume rendering of Gaussian primitives. Unlike previous approaches, DeSplat is entirely splatting-based without the need for external MLPs or pre-processing, lowering computational costs while achieving clear separation of distractors and static content. We evaluate DeSplat on a variety of real-world data sets, showcasing that it is also compatible with prior approaches using appearance MLPs and background modeling, and achieve comparable results to state-of-the-art methods.

Limitations Our method leverages view-consistency to extract as much information as possible from the images. However, if distractors appear static across most views, DeSplat may mistakenly detect them as part of the static scene. Additionally, a small color difference between distractors and static objects can hinder proper separation. Another limitation is that DeSplat may struggle to define clear boundaries for occluders, potentially leading to a loss of detail and reduced image quality. In outdoor scenes with skies and varying lighting or weather conditions, distractor Gaussians may capture these elements, making separation more challenging.

Acknowledgements

We acknowledge funding from the Research Council of Finland (grant number 339730 and 362408). MK and MT acknowledge funding from the Finnish Center for Artificial Intelligence (FAI). We acknowledge CSC–IT Center for Science, Finland, and the Aalto Science–IT project for the computational resources. Lastly, we thank Martin Trapp for helpful discussions.

References

- [1] Adam Bielski and Paolo Favaro. Emergence of object segmentation in perturbed generative models. In *Advances in Neural Information Processing Systems*, pages 7256–7266, 2019. 3
- [2] Piotr Bojanowski, Armand Joulin, David Lopez-Pas, and Arthur Szlam. Optimizing the latent space of generative networks. In *Proceedings of the 35th International Conference on Machine Learning*, pages 600–609. PMLR, 2018. 8
- [3] Jiahao Chen, Yipeng Qin, Lingjie Liu, Jiangbo Lu, and Guanbin Li. NeRF-HuGS: Improved neural radiance fields in non-static scenes using heuristics-guided segmentation. In *Proceedings of the IEEE/CVF Conference on Computer Vision and Pattern Recognition*, pages 19436–19446, 2024. 2, 6
- [4] Mickaël Chen, Thierry Artières, and Ludovic Denoyer. Unsupervised object segmentation by redrawing. In *Advances in Neural Information Processing Systems*, pages 12726–12737, 2019. 3
- [5] Xingyu Chen, Qi Zhang, Xiaoyu Li, Yue Chen, Ying Feng, Xuan Wang, and Jue Wang. Hallucinated neural radiance fields in the wild. In *Proceedings of the IEEE/CVF Conference on Computer Vision and Pattern Recognition*, pages 12943–12952, 2022. 2
- [6] Hiba Dahmani, Moussab Bennehar, Nathan Piasco, Luis Roldao, and Dzmitry Tsishkou. SWAG: Splatting in the wild images with appearance-conditioned Gaussians. In *European Conference on Computer Vision*. Springer, 2024. 2, 3, 6, 4
- [7] Kaiming He, Xiangyu Zhang, Shaoqing Ren, and Jian Sun. Deep residual learning for image recognition. In *Proceedings of the IEEE Conference on Computer Vision and Pattern Recognition*, pages 770–778, 2016. 3
- [8] Bernhard Kerbl, Georgios Kopanas, Thomas Leimkühler, and George Drettakis. 3D Gaussian splatting for real-time radiance field rendering. *ACM Transactions on Graphics*, 42(4): 139–1, 2023. 1, 2, 3, 4, 6
- [9] Shakiba Kheradmand, Daniel Rebain, Gopal Sharma, Weiwei Sun, Yang-Che Tseng, Hossam Isack, Abhishek Kar, Andrea Tagliasacchi, and Kwang Moo Yi. 3d gaussian splatting as markov chain monte carlo. In *The Thirty-eighth Annual Conference on Neural Information Processing Systems*, 2024. 4
- [10] Diederik P Kingma and Jimmy Lei Ba. Adam: A method for stochastic gradient descent. In *International Conference on Learning Representations*, 2015. 6, 3
- [11] Alexander Kirillov, Eric Mintun, Nikhila Ravi, Hanzi Mao, Chloe Rolland, Laura Gustafson, Tete Xiao, Spencer Whitehead, Alexander C Berg, Wan-Yen Lo, et al. Segment anything. In *Proceedings of the IEEE/CVF International Conference on Computer Vision*, pages 4015–4026, 2023. 2
- [12] Marcus Klasson, Riccardo Mereu, Juho Kannala, and Arno Solin. Sources of uncertainty in 3D scene reconstruction. In *European Conference on Computer Vision Workshops*. Springer, 2024. 1, 4
- [13] Jonas Kulhanek, Songyou Peng, Zuzana Kukelova, Marc Pollefeys, and Torsten Sattler. WildGaussians: 3D Gaussian splatting in the wild. In *Advances in Neural Information Processing Systems*, 2024. 2, 3, 5, 6, 7, 8, 1, 4
- [14] Zhengqi Li, Simon Niklaus, Noah Snavely, and Oliver Wang. Neural scene flow fields for space-time view synthesis of dynamic scenes. In *Proceedings of the IEEE/CVF Conference on Computer Vision and Pattern Recognition*, pages 6498–6508, 2021. 3
- [15] Yiyi Liao, Katja Schwarz, Lars Mescheder, and Andreas Geiger. Towards unsupervised learning of generative models for 3D controllable image synthesis. In *Proceedings of the IEEE/CVF Conference on Computer Vision and Pattern Recognition*, pages 5871–5880, 2020. 3
- [16] Zhixuan Lin, Yi-Fu Wu, Skand Vishwanath Peri, Weihao Sun, Gautam Singh, Fei Deng, Jindong Jiang, and Sungjin Ahn. SPACE: Unsupervised object-oriented scene representation via spatial attention and decomposition. In *International Conference on Learning Representations*, 2020. 3
- [17] Ricardo Martin-Brualla, Noha Radwan, Mehdi S. M. Sajjadi, Jonathan T. Barron, Alexey Dosovitskiy, and Daniel Duckworth. NeRF in the wild: Neural radiance fields for unconstrained photo collections. In *Proceedings of the IEEE/CVF Conference on Computer Vision and Pattern Recognition*, pages 7206–7215, 2021. 1, 2, 3, 6, 8, 4
- [18] Ben Mildenhall, Pratul P. Srinivasan, Matthew Tancik, Jonathan T. Barron, Ravi Ramamoorthi, and Ren Ng. NeRF: Representing scenes as neural radiance fields for view synthesis. *Communications of the ACM*, 65(1):99–106, 2021. 1
- [19] Michael Niemeyer and Andreas Geiger. Giraffe: Representing scenes as compositional generative neural feature fields. In *Proceedings of the IEEE/CVF Conference on Computer Vision and Pattern Recognition*, pages 11453–11464, 2021. 3
- [20] Maxime Oquab, Timothée Darcet, Theo Moutakanni, Huy V. Vo, Marc Szafraniec, Vasil Khalidov, Pierre Fernandez, Daniel Haziza, Francisco Massa, Alaaeldin El-Nouby, Russell Howes, Po-Yao Huang, Hu Xu, Vasu Sharma, Shang-Wen Li, Wojciech Galuba, Mike Rabbat, Mido Assran, Nicolas Ballas, Gabriel Synnaeve, Ishan Misra, Herve Jegou, Julien Mairal, Patrick Labatut, Armand Joulin, and Piotr Bojanowski. DINOv2: Learning robust visual features without supervision. *Transactions on Machine Learning Research (TMLR)*, 2023. 2, 3
- [21] Takashi Otonari, Satoshi Ikehata, and Kiyoharu Aizawa. Entity-NeRF: Detecting and removing moving entities in urban scenes. In *Proceedings of the IEEE/CVF Conference on Computer Vision and Pattern Recognition*, pages 20892–20901, 2024. 3
- [22] Keunhong Park, Utkarsh Sinha, Jonathan T Barron, Sofien Bouaziz, Dan B Goldman, Steven M Seitz, and Ricardo

- Martin-Brualla. Nerfies: Deformable neural radiance fields. In *Proceedings of the IEEE/CVF International Conference on Computer Vision*, pages 5865–5874, 2021. 1
- [23] Thomas Porter and Tom Duff. Compositing digital images. In *Proceedings of the 11th annual Conference on Computer Graphics and Interactive Techniques*, pages 253–259, 1984. 4
- [24] Konstantinos Rematas, Andrew Liu, Pratul P Srinivasan, Jonathan T Barron, Andrea Tagliasacchi, Thomas Funkhouser, and Vittorio Ferrari. Urban radiance fields. In *Proceedings of the IEEE/CVF Conference on Computer Vision and Pattern Recognition*, pages 12932–12942, 2022. 3
- [25] Weining Ren, Zihan Zhu, Boyang Sun, Jiaqi Chen, Marc Pollefeys, and Songyou Peng. NeRF On-the-go: Exploiting uncertainty for distractor-free NeRFs in the wild. In *Proceedings of the IEEE/CVF Conference on Computer Vision and Pattern Recognition*, pages 8931–8940, 2024. 1, 2, 5, 6, 7, 3
- [26] Robin Rombach, Andreas Blattmann, Dominik Lorenz, Patrick Esser, and Björn Ommer. High-resolution image synthesis with latent diffusion models. In *Proceedings of the IEEE/CVF Conference on Computer Vision and Pattern Recognition*, pages 10684–10695, 2022. 2, 3
- [27] Olaf Ronneberger, Philipp Fischer, and Thomas Brox. U-Net: Convolutional networks for biomedical image segmentation. In *Proceedings of the International Conference on Medical Image Computing and Computer-Assisted Intervention (MICCAI)*, pages 234–241. Springer, 2015. 3
- [28] Sara Sabour, Suhani Vora, Daniel Duckworth, Ivan Krasin, David J Fleet, and Andrea Tagliasacchi. RobustNeRF: Ignoring distractors with robust losses. In *Proceedings of the IEEE/CVF Conference on Computer Vision and Pattern Recognition*, pages 20626–20636, 2023. 1, 2, 5, 6, 7, 8, 3
- [29] Sara Sabour, Lily Goli, George Kopanas, Mark Matthews, Dmitry Lagun, Leonidas Guibas, Alec Jacobson, David J Fleet, and Andrea Tagliasacchi. SpotlessSplats: Ignoring distractors in 3D Gaussian splatting. In *European Conference on Computer Vision Workshops*, 2024. 2, 3, 5, 6, 7, 8, 1, 4
- [30] Johannes L. Schönberger and Jan-Michael Frahm. Structure-from-motion revisited. In *Proceedings of the IEEE Conference on Computer Vision and Pattern Recognition*, pages 4104–4113, 2016. 4
- [31] Noah Snavely, Steven M Seitz, and Richard Szeliski. Photo tourism: Exploring photo collections in 3D. In *ACM SIGGRAPH*, pages 835–846. 2006. 1, 2, 5, 7, 4, 6
- [32] Matthew Tancik, Vincent Casser, Xinchun Yan, Sabeek Pradhan, Ben Mildenhall, Pratul P Srinivasan, Jonathan T Barron, and Henrik Kretschmar. Block-NeRF: Scalable large scene neural view synthesis. In *Proceedings of the IEEE/CVF Conference on Computer Vision and Pattern Recognition*, pages 8248–8258, 2022. 3
- [33] Matthew Tancik, Ethan Weber, Evonne Ng, Ruilong Li, Brent Yi, Justin Kerr, Terrance Wang, Alexander Kristoffersen, Jake Austin, Kamyar Sahahi, Abhik Ahuja, David McAllister, and Angjoo Kanazawa. Nerfstudio: A modular framework for neural radiance field development. In *ACM SIGGRAPH*, 2023. 2, 5, 6, 7, 8, 1, 3, 4
- [34] Luming Tang, Menglin Jia, Qianqian Wang, Cheng Peng Phoo, and Bharath Hariharan. Emergent correspondence from image diffusion. In *Advances in Neural Information Processing Systems*, pages 1363–1389, 2023. 2
- [35] Adam Tonderski, Carl Lindström, Georg Hess, William Ljungbergh, Lennart Svensson, and Christoffer Petersson. NeuRAD: Neural rendering for autonomous driving. In *Proceedings of the IEEE/CVF Conference on Computer Vision and Pattern Recognition*, pages 14895–14904, 2024. 3
- [36] Zhou Wang, Alan C Bovik, Hamid R Sheikh, and Eero P Simoncelli. Image quality assessment: From error visibility to structural similarity. *IEEE Transactions on Image Processing*, 13(4):600–612, 2004. 3
- [37] Frederik Warburg, Ethan Weber, Matthew Tancik, Aleksander Holynski, and Angjoo Kanazawa. Nerfbusters: Removing ghostly artifacts from casually captured NeRFs. In *Proceedings of the IEEE/CVF International Conference on Computer Vision*, pages 18120–18130, 2023. 1
- [38] Tianhao Wu, Fangcheng Zhong, Andrea Tagliasacchi, Forrester Cole, and Cengiz Oztireli. D²NeRF: Self-supervised decoupling of dynamic and static objects from a monocular video. In *Advances in Neural Information Processing Systems*, pages 32653–32666, 2022. 3
- [39] Congrong Xu, Justin Kerr, and Angjoo Kanazawa. Splatfacto-W: A Nerfstudio implementation of Gaussian splatting for unconstrained photo collections. *arXiv preprint arXiv:2407.12306*, 2024. 3, 6, 7, 1, 2, 4
- [40] Jiacong Xu, Yiqun Mei, and Vishal M. Patel. Wild-GS: Real-time novel view synthesis from unconstrained photo collections. In *Advances in Neural Information Processing Systems*, 2024. 3, 6, 8, 1, 2, 4
- [41] Yunzhi Yan, Haotong Lin, Chenxu Zhou, Weijie Wang, Haiyang Sun, Kun Zhan, Xianpeng Lang, Xiaowei Zhou, and Sida Peng. Street Gaussians for modeling dynamic urban scenes. In *European Conference on Computer Vision*. Springer, 2024. 3
- [42] Yifan Yang, Shuhai Zhang, Zixiong Huang, Yubing Zhang, and Mingkui Tan. Cross-ray neural radiance fields for novel-view synthesis from unconstrained image collections. In *Proceedings of the IEEE/CVF International Conference on Computer Vision*, pages 15901–15911, 2023. 2
- [43] Ziyi Yang, Xinyu Gao, Wen Zhou, Shaohui Jiao, Yuqing Zhang, and Xiaogang Jin. Deformable 3D Gaussians for high-fidelity monocular dynamic scene reconstruction. In *Proceedings of the IEEE/CVF Conference on Computer Vision and Pattern Recognition*, pages 20331–20341, 2024. 3
- [44] Raza Yunus, Jan Eric Lenssen, Michael Niemeyer, Yiyi Liao, Christian Rupprecht, Christian Theobalt, Gerard Pons-Moll, Jia-Bin Huang, Vladislav Golyanik, and Eddy Ilg. Recent trends in 3D reconstruction of general non-rigid scenes. In *Computer Graphics Forum*, page e15062. Wiley Online Library, 2024. 3
- [45] Dongbin Zhang, Chuming Wang, Weitao Wang, Peihao Li, Minghan Qin, and Haoqian Wang. Gaussian in the wild: 3D Gaussian splatting for unconstrained image collections. In *European Conference on Computer Vision*, pages 341–359. Springer, 2024. 2, 3, 6, 4
- [46] Xinjie Zhang, Xingtong Ge, Tongda Xu, Dailan He, Yan Wang, Hongwei Qin, Guo Lu, Jing Geng, and Jun Zhang.

GaussianImage: 1000 FPS image representation and compression by 2D Gaussian splatting. In *European Conference on Computer Vision*, pages 327–345, 2024. [3](#)

- [47] Hongyu Zhou, Jiahao Shao, Lu Xu, Dongfeng Bai, Weichao Qiu, Bingbing Liu, Yue Wang, Andreas Geiger, and Yiyi Liao. HUGS: Holistic urban 3D scene understanding via Gaussian splatting. In *Proceedings of the IEEE/CVF Conference on Computer Vision and Pattern Recognition*, pages 21336–21345, 2024. [3](#)
- [48] Xiaoyu Zhou, Zhiwei Lin, Xiaojun Shan, Yongtao Wang, Deqing Sun, and Ming-Hsuan Yang. DrivingGaussian: Composite Gaussian splatting for surrounding dynamic autonomous driving scenes. In *Proceedings of the IEEE/CVF Conference on Computer Vision and Pattern Recognition*, pages 21634–21643, 2024. [3](#)

DeSplat: Decomposed Gaussian Splatting for Distractor-Free Rendering

Supplementary Material

A. Method Details

Here, we provide additional details about DeSplat. In general, DeSplat follow the same settings as Splatfacto from Nerfstudio [33], *e.g.*, utilizing a warm-up phase as 500 steps and image downscaling factor as 2 at the beginning of training. We present modifications that improved the separation of static elements and distractors next by disabling opacity reset and modifying the color representation. Additionally, we describe how we combine DeSplat with the appearance modeling in [13] and the background model in [39] which we use in the Photo Tourism experiments.

Disabling Opacity Reset for Distractor Gaussians Kerbl et al. [8] introduced an opacity reset mechanism in 3DGS that removes Gaussian points located very close to the camera. However, we only apply the opacity reset on static Gaussians and disable it for the distractor Gaussians, as it can cause confusion between occluders and static objects.

RGB Color Representation for Distractor Gaussians We modify the color representation for the distractor Gaussians to model the color in RGB space and use clamping to set its range instead of using a sigmoid function. Modeling the colors as RGB vectors instead of using SH coefficients alleviates the need to compensate for view-dependent effects using SH as the distractor Gaussians are per-view. Additionally, applying clamping into the range $[0, 1]$ of the RGB colors instead of using a sigmoid function enabled better learning of distractors with colors at the extremes white (1) and black (0).

Appearance Embeddings We show that DeSplat can be combined with MLPs for modeling appearance variations with per-view image embeddings. This is commonly used for NeRF [17] and 3DGS [13, 29, 39, 40] in the Photo Tourism data set which consists of web images with varying resolutions, weather conditions, and lighting scenarios. We follow the appearance modeling by Kulhanek et al. [13], which use per-image embeddings $\{\mathbf{e}_j\}_{j=1}^{N_{\text{train}}}$ with N_{train} as the number of training images to handle varying appearances and illuminations, and per-Gaussian embeddings $\{\mathbf{z}_i\}_{i=1}^N$ to handle varying colors for each Gaussian under different appearances. The per-image embeddings $\mathbf{e}_j \in \mathbb{R}^{d_e}$, per-Gaussian embeddings $\mathbf{z}_i \in \mathbb{R}^{d_z}$, and the 0-th order SH coefficient $\bar{\mathbf{c}}_i$ are input to an MLP f_ϕ as

$$(\beta, \gamma) = f_\phi(\mathbf{e}_j, \mathbf{z}_i, \bar{\mathbf{c}}_i), \quad (6)$$

where $\beta, \gamma \in \mathbb{R}^3$ are the shift and scale of an affine transformation respectively, and ϕ are the parameters of the MLP.

The view-dependent color of the i -th Gaussian \mathbf{c}_i is then toned as

$$\tilde{\mathbf{c}}_i = \gamma \odot \mathbf{c}_i + \beta, \quad (7)$$

where \odot is an element-wise multiplication. The toned color $\tilde{\mathbf{c}}_i$ is then passed to the rasterization. In App. B, we show the results for DeSplat on Photo Tourism where we apply the appearance modeling on the static Gaussians.

Background Model For background modeling, we follow the approach introduced in Splatfacto-W [39]. Instead of previous methods that use a unified color for the background, we leverage the same per-image embeddings used for appearance modeling to predict the Spherical Harmonics (SH) coefficients b for the background using an MLP. Prior to applying alpha blending, we render the background RGB color \mathbf{c}_{BG} from the predicted SH coefficients.

$$b = f_{\text{BG}}(\mathbf{e}_j) \quad (8)$$

To encourage the Gaussians correspondent to these areas to be low, we also apply the opacity regularization from Splatfacto-W [39] for both distractor Gaussians and static Gaussians.

$$\mathcal{L}_{\text{bg}} = \sum_{\mathbf{r} \in \mathcal{P}} |\alpha_d(\mathbf{r}) + (1 - \alpha_d(\mathbf{r})) \cdot \alpha_s(\mathbf{r})| \quad (9)$$

where $\alpha(\mathbf{r})$ is the per-pixel accumulation of the Gaussians at pixel \mathbf{r} . The set \mathcal{P} is defined as $\mathcal{P} = \{\mathbf{r} \mid M(\mathbf{r}) > 0.6\}$.

Similar to Splatfacto-W [39], we also use a per-pixel mask M to filter the area that the error of predicted background color and ground truth $\epsilon(\mathbf{r})$ is smaller than a threshold \mathcal{T}_ϵ , with a box filter $\mathcal{B}_{3 \times 3}$ to force the smoothness on the background

$$\tilde{\epsilon}(\mathbf{r}) = \epsilon(\mathbf{r}) \leq \mathcal{T}_\epsilon, \quad (10)$$

$$M(\mathbf{r}) = (\tilde{\epsilon}(\mathbf{r}) * \mathcal{B}_{3 \times 3}). \quad (11)$$

The final loss function of our method on Photo Tourism data set is:

$$\mathcal{L} = \mathcal{L}_{\text{GS}} + \lambda_d \alpha_d + \lambda_{\text{bg}} \mathcal{L}_{\text{bg}} \quad (12)$$

B. Additional Experiments

B.1. Data Sets

RobustNeRF [28] We run experiments on all five scenes *Statue*, *Android*, *Crab (1)*, *Crab (2)*, and *Yoda*. All images are downscaled $8 \times$ as instructed in [28]. The scenes are indoor and are captured under different occluder settings.

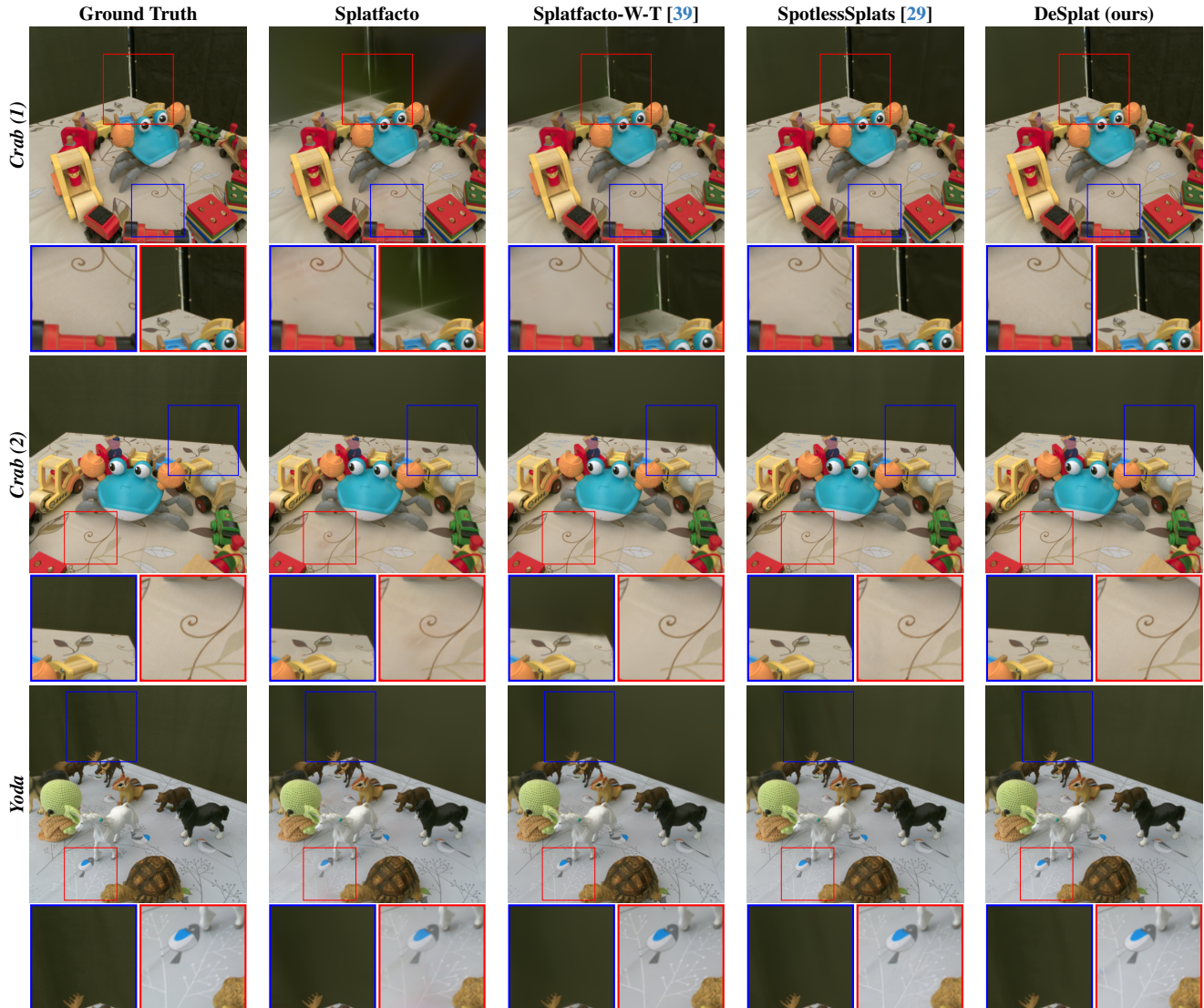


Figure A10. **Additional qualitative results on the RobustNeRF data set [28].** In the *Crab (1)*, *Crab (2)* and *Statue* scenes, DeSplat reconstructs static objects and backgrounds accurately.

The *Crab(2)* and *Yoda* scenes include both clean and cluttered image variants from the same viewpoint, enabling us to perform ablation studies by varying the ratio of clean to cluttered training images (see Fig. 9(left)).

On-the-go [25] We run experiments on the scenes *Mountain*, *Fountain*, *Corner*, *Patio*, *Spot*, and *Patio-High* that are commonly used for reporting quantitative performance metrics [13, 25, 29]. These scenes are further categorized according to three different occlusion rates: low (*Mountain*, *Fountain*), medium (*Corner*, *Patio*), and high (*Spot*, *Patio-High*) occlusion. All images are downscaled $8\times$, except the *Patio* scene which is downscaled $4\times$. Furthermore, we use *Arc de Triomphe* for visualization purposes (see Fig. 4).

Photo Tourism [31] We run experiments on the scenes

Brandenburg Gate, *Sacre Coeur*, and *Trevi Fountain* that are commonly used for reporting quantitative performance metrics [6, 13, 39, 40, 45]. The images for these scenes are complex, exhibiting different resolutions and varying illumination and weather effects, which necessitates view-dependent appearance modeling [17]. We follow the evaluation protocol from Martin-Brualla et al. [17] where a per-image embedding is optimized on the left half of the evaluation image and then evaluated on its right half. Furthermore, we follow the test-time optimization used by Kulhanek et al. [13] to optimize the per-image embeddings for the evaluation images. Table A5 shows the reported metrics for the three scenes.

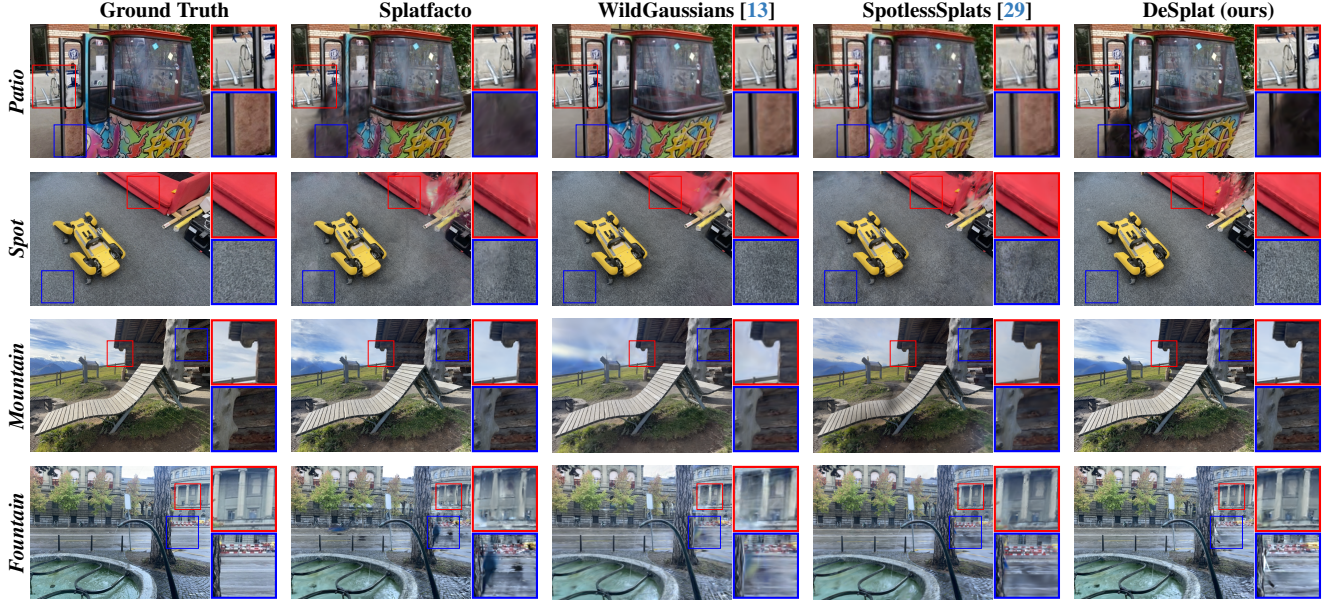


Figure A11. Additional qualitative results on On-the-go data set [25].

B.2. Baselines

For all baselines, except Splatfacto and Splatfacto-W, we compare the performance of DeSplat against the PSNR, SSIM, and LPIPS metrics that was reported in their corresponding works to ensure consistency. For Splatfacto and Splatfacto-W, we run experiments for these using `gsplat` version 1.0.0 and `nerfstudio` version 1.1.4.

For the qualitative results, we run experiments with SpotLessSplats [29] and WildGaussians [13] to obtain visualizations (e.g., see Fig. 6). We run SpotLessSplats using the reimplementation¹ in the `gsplat` library (version 1.1.1). For WildGaussians, we use the official code-base and trained model checkpoint files for evaluation and qualitative images.

B.3. Implementation Details

We base our implementation of DeSplat on Nerfstudio code-base [33] (`nerfstudio` version 1.1.4 and `gsplat` version 1.0.0). For a fair comparison of computational efficiency, all ablation experiments are conducted on a single NVIDIA GeForce RTX 2060 SUPER GPU. Next, we present the hyperparameters used for the data sets.

RobustNeRF and On-the-go We use the same hyperparameter settings for DeSplat on the scenes from RobustNeRF [28] an On-the-go [25] data sets. More specifically, we follow the default hyperparameter setting for Splatfacto [33] and train for 30k iterations. Densification of distractor Gaussians stops after 15k iteration. We initialize 1000 distractor points in every training image (see Sec. 3.1 for details) and

¹<https://github.com/lilygoli/SpotLessSplats/tree/main>

initialize the static points using the standard method based on the COLMAP point cloud, as employed in Splatfacto. All parameters of static and distractor points are optimized using Adam optimizer [10]. For the distractor points, we set the learning rates for the quaternions, scales and RGB colors to 0.01, 0.05 and 0.025 respectively, while the learning rates are kept as the Splatfacto default for the means and opacities. The regularization on the alpha-blending weights are set to $\lambda_d = 0.01$ and $\lambda_s = 0.01$ in the loss in Eq. (5).

Photo Tourism We train each scene for 200k iterations. We employ the appearance modeling from WildGaussians [13] which uses an MLP with 2 hidden layers of size 128. The per-image embedding $\mathbf{e}_j \in \mathbb{R}^{d_e}$ has dimension of $d_e = 32$, while the per-Gaussian embedding $\mathbf{z}_i \in \mathbb{R}^{d_z}$ has dimension $d_z = 24$ and is initialized using Fourier frequencies with 4 components. All parameters above are optimized using Adam optimizer [10] with learning rate 0.0005 for the MLP, 0.001 for the per-image embeddings \mathbf{e}_j and 0.005 for the per-Gaussian embeddings \mathbf{z}_i .

For background modeling, we use the background MLP from [39] consisting of 3 hidden layers with 128 hidden units each. The Spherical Harmonics (SH) degree of the background model is set to 4. The learning rates for the background model encoder and the 0th-order SH prediction head are 0.002, while the learning rate for the remaining SH orders is set to 0.0001. The Adam optimizer is used, along with an Exponential decay scheduler with decay rates of 0.0001, 0.0002, and 0.00001 separately. The regularization weights are configured as follows: $\lambda_s = 0$, $\lambda_d = 0.01$, and $\lambda_{bg} = 0.15$. The threshold \mathcal{T}_ϵ for regularization is set to 0.003. All other settings are kept consistent with the

Table A5. **Performance comparison between our method and the baselines on the Photo Tourism data set [31].** The **first**, **second**, and **third** values are highlighted. DeSplat perform significantly better than Splatfacto, indicating that the explicit scene separation is useful for these scenes.

| Method | Brandenburg Gate | | | Sacre Coeur | | | Trevi Fountain | | |
|---------------------------|------------------|-----------------|--------------------|-----------------|-----------------|--------------------|-----------------|-----------------|--------------------|
| | PSNR \uparrow | SSIM \uparrow | LPIPS \downarrow | PSNR \uparrow | SSIM \uparrow | LPIPS \downarrow | PSNR \uparrow | SSIM \uparrow | LPIPS \downarrow |
| Splatfacto [33] | 19.50 | 0.885 | 0.183 | 17.15 | 0.831 | 0.210 | 17.63 | 0.696 | 0.334 |
| Splatfacto-W [39] | 26.87 | 0.932 | 0.124 | 22.53 | 0.876 | 0.158 | 22.66 | 0.769 | 0.224 |
| Splatfacto-W-A [39] | 27.50 | 0.930 | 0.130 | 22.62 | 0.876 | 0.156 | 22.81 | 0.770 | 0.228 |
| Splatfacto-W-T [39] | 26.16 | 0.925 | 0.131 | 22.78 | 0.878 | 0.155 | 22.88 | 0.772 | 0.228 |
| SWAG [6] | 26.33 | 0.929 | 0.139 | 21.16 | 0.860 | 0.185 | 23.10 | 0.815 | 0.208 |
| GS-W [45] | 27.96 | 0.932 | 0.086 | 23.24 | 0.863 | 0.130 | 22.91 | 0.801 | 0.156 |
| Wild-GS [40] | 29.65 | 0.933 | 0.095 | 24.99 | 0.878 | 0.127 | 24.45 | 0.808 | 0.162 |
| WildGaussians [13] | 27.77 | 0.927 | 0.133 | 22.56 | 0.859 | 0.177 | 23.63 | 0.766 | 0.228 |
| DeSplat (ours) - A | 26.72 | 0.918 | 0.132 | 22.28 | 0.876 | 0.159 | 23.06 | 0.774 | 0.229 |
| DeSplat (ours) | 25.04 | 0.920 | 0.142 | 20.14 | 0.868 | 0.178 | 23.31 | 0.775 | 0.226 |

parameters used for the On-the-go and RobustNerf datasets.

We also perform an ablation study using only the appearance embedding model while disabling the background model, which is denoted as DeSplat-A. In this ablation, the learning rates and MLP structure for the appearance embedding model are kept the same as described above, while the regularization weights are set as follows: $\lambda_s = 0.01$, $\lambda_d = 0.01$, and $\lambda_{bg} = 0$.

We follow the evaluation protocol [13, 17] and learn the per-image appearance embedding of a test image. During the test phase, we train only the per-image appearance embedding for 128 iterations using the Adam optimizer with a learning rate of 0.01. All other parameters remain frozen during this period. We only learn the embedding on the left half of the image, and then evaluate the right half after the optimization process.

B.4. More Qualitative Results

Comparison on RobustNeRF data set We present the qualitative results for the *Crab (1)*, *Crab (2)*, and *Yoda* scenes from the RobustNeRF dataset. Our method achieves state-of-the-art results across all three scenes. However, we observe that our occluder removal does not always outperform all baselines. In some cases, where other baselines successfully remove occluders completely, our method occasionally leaves small artifacts. Despite this, our approach excels in reconstructing the background with exceptional clarity. More details see Fig. A10.

Comparison on On-the-go data set We also compare our method with other baselines on the *Patio*, *Spot*, *Mountain*, and *Fountain* scenes from the On-the-go dataset. In the *Patio* scene, our DeSplat does not perform well, as it fails to remove all occluders effectively. This is due to a person wearing a black jacket standing in one place for a long period, resulting in black artifacts. For detailed analysis, see the failure analysis section App. B.6. In the *Spot* scene, DeSplat produces fewer artifacts and reconstructs more detailed background information. As shown in Fig. A11, our

method achieves finer reconstruction on the floor, and the wrinkles on the sofa closely resemble the ground truth. In the *Mountain* scene, our method better reconstructs the global color and texture, especially for the wooden hut. Outside of the zoomed-in areas, white artifacts in the bottom-right corner and black artifacts on the chair, which are visible in SpotlessSplats, are not present in our results. However, our method has difficulty reconstructing the sky, as moving clouds are sometimes incorrectly identified as dynamic elements. More details can be found in B.6. In the *Fountain* scene, while none of the baselines can fully remove artifacts near the trunk, our method successfully reconstructs the column of the background architecture.

Comparison on Photo Tourism data set We evaluate our method on the *Brandenburg Gate*, *Sacre Coeur*, and *Trevi Fountain* scenes from the Photo Tourism data set, comparing it with the baselines. As shown in Table A5, after incorporating appearance embeddings, our DeSplat outperforms some baselines and achieves results close to the state-of-the-art. However, the metrics slightly degrade when incorporating background modeling, which aligns with the results of Splatfacto-W. Removing background Gaussians results in the loss of high-frequency details in the background, which reduces image quality. Moreover, it remains challenging to fully separate the background sky from the foreground, adding complexity to scene reconstruction. The gap between our method and the baselines is smallest for the *Trevi Fountain* scene, as in this scene, the distribution of distractors in the training images is relatively concentrated, making it easier for our method to learn dynamic elements effectively. From Fig. A12, our method produces visually appealing results with appearance embeddings, reconstructing fine details and achieving a smoother background compared to Splatfacto-W and WildGaussians.

B.5. Computational Efficiency

In Table A6, we compare our rendering speed (FPS), memory usage (MB), and training time (min) for DeSplat, Splatfacto, and SLS-mlp [29]. We also include the memory usage

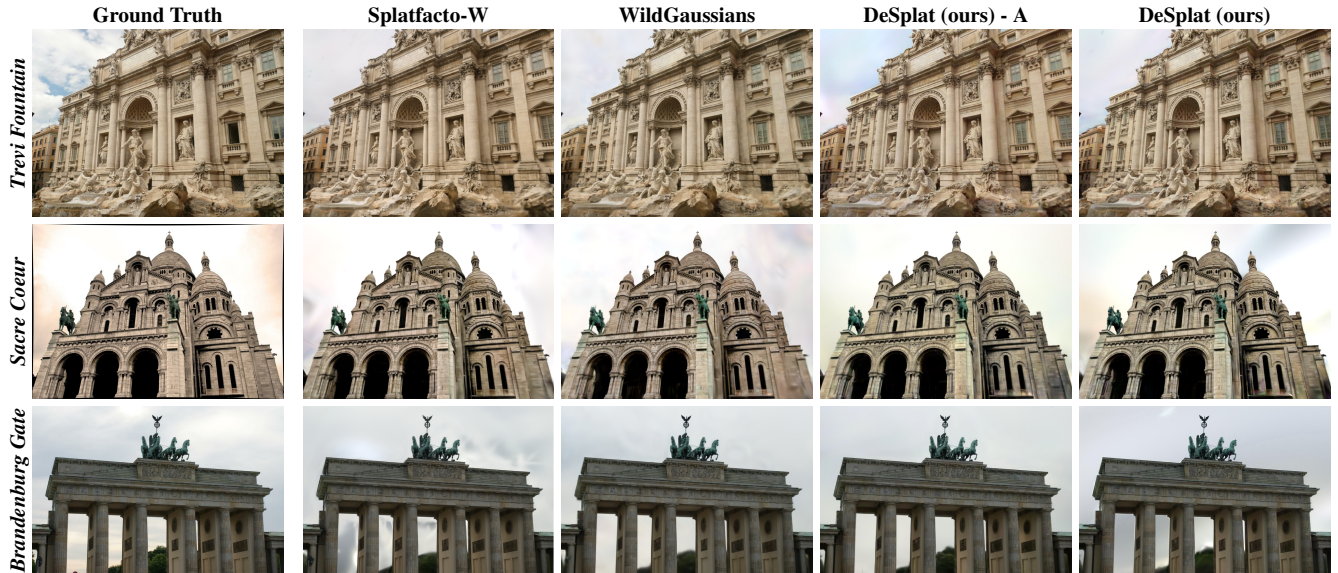


Figure A12. **Qualitative results on the Photo Tourism data set** [31]. including Our method demonstrates high rendering quality in the *Trevi Fountain*, *Brandenburg Gate*, and *Sacre Coeur* scenes.

to store the distractor Gaussians for DeSplat. The FPS is reported using the `ns-eval` in Nerfstudio [33] which calculates the FPS using both the rendering time and evaluation time (including PSNR, SSIM, LPIPS). We observe that DeSplat achieves similar rendering speed comparable to vanilla Splatfacto due to DeSplat being a pure splatting method. DeSplat results in a slight memory overhead compared to Splatfacto, however, note that only the static Gaussians need to be kept for novel view synthesis. Training time increases by a few minutes due to the increased memory usage. Finally, we observe that DeSplat is faster, more memory efficient, and requires less training time than SLS-mlp.

Table A6. **Computational efficiency.** Comparison of rendering speed (FPS), memory size (MB), and training time (min) for DeSplat, Splatfacto, and SLS-mlp [29] on *Statue* and *Android* scene [28]. Dist. Size denotes the memory required for distractor Gaussians. DeSplat achieve similar FPS as Splatfacto while increasing size and training time slightly.

| Scene | Method | Render Speed (FPS) | Size (MB) | Dist. Size (MB) | Training Time (min) |
|---------|--------------|--------------------|-----------|-----------------|---------------------|
| Statue | Splatfacto | 106.34 | 38.58 | - | 9:41 |
| | SLS-mlp [29] | 12.50 | 112.94 | - | 29:59 |
| | Ours | 108.92 | 47.05 | 16.80 | 13:05 |
| Android | Splatfacto | 104.24 | 51.94 | - | 10:03 |
| | SLS-mlp [29] | 11.36 | 133.12 | - | 27:01 |
| | Ours | 106.58 | 66.58 | 18.33 | 14:14 |

B.6. Failure Cases

Our DeSplat performs well, particularly in scenarios with minimal changes in lighting and weather, and where occluders vary across camera views, such as in the *Yoda* and *Crab* scenes. However, its performance decreases in outdoor datasets with complex lighting and weather variations, be-

cause without the help of appearance embedding, the occluders may also explain part of the background. For example, in *Mountain* scene, the cloud at sky is not identical in every frame, leading some of the distractor Gaussians explain the cloud and sky. Another limitation arises when occluders persist across many frames. Since our method separates distractors based on photometric inconsistencies between views, occluders that remain in the same or similar positions across multiple frames are misclassified as static objects. A notable example is the *Patio* scene. Consequently, as illustrated in Fig. A13 for reference.

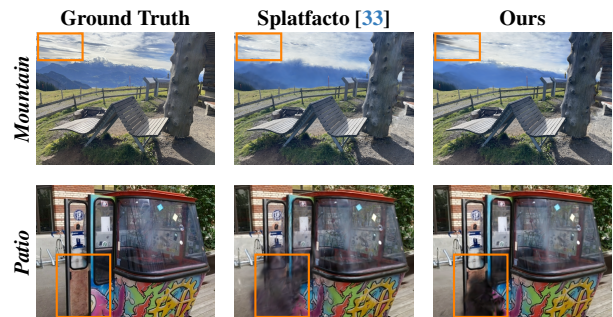


Figure A13. **Failed Cases in the Mountain and Patio Scenes.** The upper-left corner of the *Mountain* scene reveals a visible hole, while the black artifacts in the *Patio* scene appear denser compared with Splatfacto.

C. Future Directions

Investigating how to combine appearance modeling with the decomposed Gaussians for separation and better controlla-

bility is a key next step to improve DeSplat’s applicability for large-scale 3D reconstruction tasks [31]. Since DeSplat is a pure splatting method, an interesting future direction is to incorporate semantic features from foundation models for improving the separation between static objects and distractors, which has shown to effectively remove distractors in 3DGS [13, 29]. Additionally, informing the initialization step of the distractor Gaussians with plausible spatial locations and shapes of the occluders, and assigning Gaussian sets per occluder could potentially yield a more fine-grained scene decomposition. We hope that this work can spur more research for explicit 3D scene decomposition based on 3DGS.